Accurate Computation of Fracture Density Variations: A New Approach Tested on Fracture Corridors

Sophie Viseur, Juliette Lamarche, Clément Akriche, Sébastien Chatelée, Metzger Mombo Mouketo, Bertrand Gauthier

Accurate Computation of Fracture Density Variations: A New Approach Tested on Fracture Corridors

Sophie Viseur[1], Juliette Lamarche[1], Clément Akriche[2], Sébastien Chatelée[2], Metzger Mombo Mouketo[2], Bertrand Gauthier[3]

Abstract Fracture density is an important parameter for characterizing fractured reservoirs. Stochastic object-based simulation algorithms that generate fracture networks commonly rely on a fracture density to populate the reservoir zones with individual fracture surfaces. Reservoirs, including fracture corridors, represent particular challenges in petroleum reservoir studies. Indeed, it is difficult to identify fracture corridor zones objectively and precisely along one-dimensional well data, which are characterized by high fracture densities compared to diffuse fractures. To estimate fracture density, a common practice is to graphically depict only fracture corridors on fracture cumulative intensity curves. In this paper, an approach is proposed to formalize this technique using hypothesis testing. This method precisely compartmentalizes the well data into several zones having specific fracture densities. The method consists of the following steps: (i) dividing the diagram into zones depending on *a priori* drastic changes in density, (ii) computing the local accurate fracture density for each zone and (iii) clustering the zones characterized by similar densities statistically. The key point is to couple regression and hypothesis testing. The regression aims at computing local average fracture density and the hypothesis testing aims at clustering zones for which the densities are statistically the most similar. The proposed approach is dedicated to one-dimensional fracture surveys, such as well data and outcrop scanlines. First, a synthetic case study is presented to prove the ability to highlight changes in fracture

✉ Sophie Viseur
viseur@cerege.fr

1 CNRS, IRD, INRAE, Coll France, CEREGE, Aix Marseille University, 13545 Aix-en-Provence, France

2 Aix Marseille University, 3 Place Victor Hugo, 13331 Marseille cedex 03, France

3 Total EP, Tour Coupole, 2 Place Jean Millier, La Défense 6, 92078 Paris-La Défense Cedex, France

density. Second, the procedure is applied on a scanline dataset collected in a quarry (Calvisson, SE France) to show the usefulness of characterizing fracture corridors.

Keywords Fracture density · Hypothesis testing · Regression · Classification · Fracture corridor

1 Introduction

Fractures have major impacts on fluid flow in most types of tight reservoirs (Antonellini and Aydin 1994; Gauthier et al. 2000; Hansford and Fishe 2009; Agosta et al. 2010). Many geostatistical approaches have been proposed to model three-dimensional fracture networks (Chilès 1988; Bonneau et al. 2013). These geostatistical methods generally require inputs such as fracture sizes, orientations and densities. Fracture abundance, termed as Pij, has been defined (Dershowitz 1984; Dershowitz and Herda 1992; Gauthier et al. 2012) so that i is the dimension of the sampling zone (1=lines, 2=areas, 3=volumes) and j is the dimension of the measured features (0=number, 1=length, 2=area, 3=volume). $P30$ or $P32$ (Gauthier et al. 2012) is required for geostatistical approaches but they are generally difficult to estimate from subsurface data because only wells, which are one-dimensional data, allow fractures to be observed. Approaches have been proposed to determine $P10$ or $P32$ by considering assumptions (Barthélémy et al. 2009; Kherroubi and Etchecopar 2009), and sizes from well fracture observations (Gauthier et al. 2012; Gillespie et al. 1993; Marrett et al. 2018) or logs (Tokhmchi et al. 2010). As the fracture density may vary spatially depending on contextual factors (e.g., lithology, stress constraints), its stationarity is then often questioned before modeling fracture networks. For instance, different facies may lead to different fracture densities, and among fractures, corridors are peculiar geological features characterized by sudden increases of fracture density (Ray et al. 2012; Chatelée et al. 2015). A variety of methods have been proposed to characterize the spatial organization of fractures including the fracture spacing index (Narr and Suppe 1991), the coefficient of variation (Gillespie et al. 1999) or more recently, the lacunarity, a non scale-dependent entity (Roy et al. 2010, 2014), to identify fracture clusters due to a particular process, such as fracture corridors, from random clusters. However, these methods only estimate the existing pattern types (cluster, random, fractal, etc.) and sizes within the fracture networks, but not their locations. They also do not estimate the fracture density or perform statistical comparisons between fracture densities to decipher whether two zones share the same density statistically. Alternatively, fracture cumulative intensity (FCI) curves, which plot the cumulative fracture intensity versus the distance to a datum, have been used to graphically define sudden changes in fracture density (Dezayes et al. 2005; Fox et al. 2007; Jambayev 2013; Emiliano et al. 2016) but no formal mathematical method is known to statistically compare or cluster fracture density values.

In this paper, an approach, based on the FCI curves, is proposed to estimate $P10$ from well data or outcrop scanlines and to statistically compare computed values. Depending on a curvature-based criterion, the diagram is sequentially split into several zones, in which simple regression is used to estimate the fracture density. Hypothesis

testing allows the computation of the distance between the estimated per-zone $P10$. This distance is used in a clustering algorithm to gather zones with similar fracture densities. In the first section, basics on statistical methods are presented. The approach proposed to estimate $P10$ is described in the second section. The presented automated clustering of zones sharing similar fracture densities can be applied to several issues (e.g., facies-dependent fracture densities, comparisons between data sources (Souche et al. 2016)) but, in this paper, it is used for highlighting fracture corridors. Finally, results on synthetic and real case studies (Calvisson, Nîmes, France) are presented and discussed.

2 Basics on Statistical Tools

The simple regression (SR) may be used to linearly model the relationship between two variables (Eisenhauer 2003). A key output is the slope of the linear trend between both variables. Depending on the used regression model, the slopes computed from two independant samplings of these two variables may be statistically tested with hypothesis testing. The hypothesis testing assesses whether the estimated slopes are to be considered as similar (i.e., stemming from the same statistical population) or not. Furthermore, clustering algorithms are alternative techniques to cluster samples that share similar properties. These techniques are used in the proposed approach; see below for brief description.

2.1 Simple Regression with Intercepts

Let us assume two variables X and Y are measured on a n-sampling. The linear regression model of Y on X is written as follows (Fig. 1)

$$y_i = a \cdot x_i + b + \epsilon_i, i \in [1; n], \tag{1}$$

with (x_i, y_i) the pairwise values measured at datapoints, a the slope and b the intercept of the linear model, and ϵ_i is the random part non-explained by the linear model. Various fitting models may be chosen to determine a and b. The most common one is

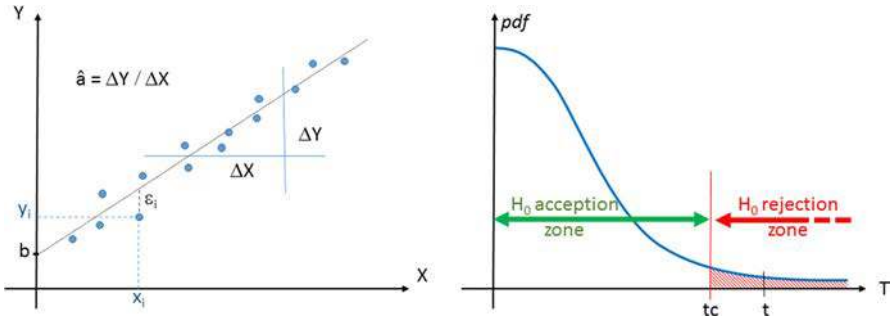

Fig. 1 Statistical methods. Left: linear regression; right: hypothesis testing

the least-mean-squares (LMS) technique, commonly termed as model I. Using model I means that the variable X *a priori* explains Y, or contains no error (i.e., X is the controlled variable). The model II includes Major Axis and is recommended when both variables contain errors or if there is *a priori* no evident causal relationship between the variables. In this paper, LMS was used and only this model is considered in the following sections.
Using the LMS, $\hat{a}$ and $\hat{b}$ are estimated as follows (Saporta 1997)

$$\hat{a} = \frac{\sum_{i=1}^{n}(y_i-\bar{y})(x_i-\bar{x})}{\sum_{i=1}^{n}(x_i-\bar{x})^2} \; and \; \hat{b} = \bar{y} - \hat{a} \cdot \bar{x} \; . \tag{2}$$

Also, it is a common practice to compute the coefficient of determination R^2, which accounts for the dispersion of the (x_i, y_i) pairwise values around the linear trend. $R^2 \in [0; 1]$ is considered as a quality criterion of the linear model if it is close to 1. However, additional analyses (e.g., analyses of residuals as well as the slope and intercept significances) are often needed (Saporta 1997).

2.2 Comparison of Regression Slopes Between Two Independent Samplings

Let X and Y be variables measured on two independent samples $\{x_i, y_i\}_{i\in[1;n_1]}$ and $\{x_j, y_j\}_{j\in[1;n_2]}$, respectively. Let us assume that $\hat{a}_1$ and $\hat{a}_2$ were computed by SR using LMS of Y onto X. The aim is to determine whether the theoretical slopes a_1 and a_2 may be statistically considered as equal, which corresponds to the following hypothesis testing

$$\begin{cases} H_0 : a_1 = a_2 \\ H_1 : a_1 \neq a_2 \end{cases} . \tag{3}$$

The statistical test is based on the computation of the statistics t that should follow the Student law with $n_1 + n_2 - 4$ degrees of freedom

$$t = \frac{a_1 - a_2}{\sqrt{s_{a_1}^2 + s_{a_2}^2}} \sim T(n_1 + n_2 - 4), \tag{4}$$

with

$$\begin{aligned} s_{a_1}^2 &= \frac{1/(n_1-2).\sum_{i=1}^{n_1}(y_i-\hat{y_i})^2}{\sum_{i=1}^{n_1}(x_i-\bar{x})^2} \\ s_{a_2}^2 &= \frac{1/(n_2-2).\sum_{j=1}^{n_2}(y_i-\hat{y_i})^2}{\sum_{j=1}^{n_2}(x_j-\bar{x})^2} \\ \hat{y_i} &= \hat{a}.x_i + \hat{b} \end{aligned} \; . \tag{5}$$

Any hypothesis testing is based on the user-defined risk α to reject H_0 although it is true (Fig. 1). Thus, depending on n_1, n_2 and α, the critical value t_c is determined from the Student Law $T(n_1+n_2-4)$ (Saporta 1997). The observed statistics $\hat{t}$ is estimated from the estimated slopes $\hat{a}_1$ and $\hat{a}_2$, using Eq. 4. Using bilateral hypothesis testing, the result is given as follows (Fig. 1): if $\hat{t} > t_c$, the slopes a_1 and a_2 are considered as significantly different; if $\hat{t} \leq t_c$, the slopes a_1 and a_2 are considered as similar.

2.3 Hierarchical Ascendant Clustering

Clustering algorithms aim to gather samples sharing the same properties into clusters (Saporta 1997). Among the clustering techniques, hierarchical ascendant clustering (HAC) is used whenever the *a priori* number of clusters is unknown, hence an optimal partition of the sampling must be sought. HAC relies on a measure of distance or dissimilarity, but also on an aggregation criterion (e.g., complete link, Ward). The Ward criterion requires a Euclidian distance, while other criteria do not impose such a condition.

At the beginning, each sample is considered as an individual cluster and, at each step of clustering, the two closest clusters according to the used distance and aggregation criterion are merged. These successive operations are summarized in the dendrogram. The dendrogram is the tree of merging steps, which is plotted as a function of the aggregation rate. The height of the tree branches is the aggregation gap. The optimal partition is chosen considering the maximum gap value in the dendrogram, as suggested by Saporta (1997). Moreover, it is common to consider the second maximum gap when the maximum gap splits only two groups (Saporta 1997). Indeed, the splitting into two groups often leads to an important increase in inter-class variance (due to outliers, etc.).

3 Proposed Approach for Computing $P10$

In this section, it is supposed that one-dimensional data of fracture locations have been collected along wells or scanlines, and that the Terzaghi corrections (Terzaghi 1964) have been previously applied. First, the mathematical settings and the concept of our approach to characterize $P10$ spatial variability or stationarity are described. Second, the approach to estimate $P10$ in the stationary case is presented. Finally, a semi-automated method is proposed to isolate zones where fracture density is roughly stationary, which will allow us to estimate $P10$ in each zone and to cluster zones sharing similar $P10$ values. The latter section is particularly dedicated to characterizing the fracture corridor occurrence and boundaries.

3.1 Settings and Key-Points

Let F and D be two random variables that correspond to the fracture rank along a linear sampling and to the distance from the first fracture, respectively. Considering this data type, F corresponds to values $f_i = i$ with $i \in [1; N_f]$, where N_f is the total number of fractures and D is defined by $\{d_i\}_{i\in[1;N_f]}$ with $d_1 = 0$ (Fig. 2).

If F and D are plotted in a diagram (Fig. 2), it could be deduced that the derivative of F with respect to D corresponds to $P10$. Indeed, the approximation of the derivative between two samples i and j can be written as follows

$$\frac{\Delta F}{\Delta D} = \frac{f_j - f_i}{d_j - d_i} = \frac{j - i}{d_j - d_i}, \tag{6}$$

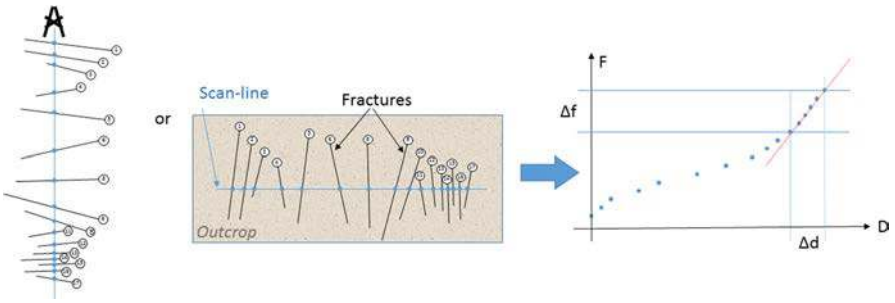

Fig. 2 Data representation. Left: well data or scanline on outcrop; right: diagram between F and D

where $d_j - d_i$ represents the distance between the fractures i and j and $f_j - f_i = j - i$ corresponds to the number of fractures over $d_j - d_i$. Therefore, this entity corresponds to a fracture density $P10$ (i.e., the number of fractures counted over a distance).

This formulation and the shape of the (F, D) plot (Fig. 3) leads to the three following key-points: (i) the straighter the (F, D) plot is, the more constant (i.e., stationary) $P10$ is over the studied length (Fig. 3a, b). The slope of the linear trend is an estimation of $P10$; (ii) if the (F, D) plot shows discontinuities or "sharp angles", this means that $P10$ changes abruptly, which highlights fracture corridor boundaries (Fig. 3c); (iii) if the (F, D) plot shows an exponential-like increase, this means that $P10$ evolves gradually (Fig. 3d).

Thus, characterizing the shape of the (F, D) graph yields the ability to characterize the spatial fracture density variability. In case of linear trend (first abovementioned key-point), the aim is to estimate the fracture density by computing the slope of the linear trend that best fits the (F, D) graph.

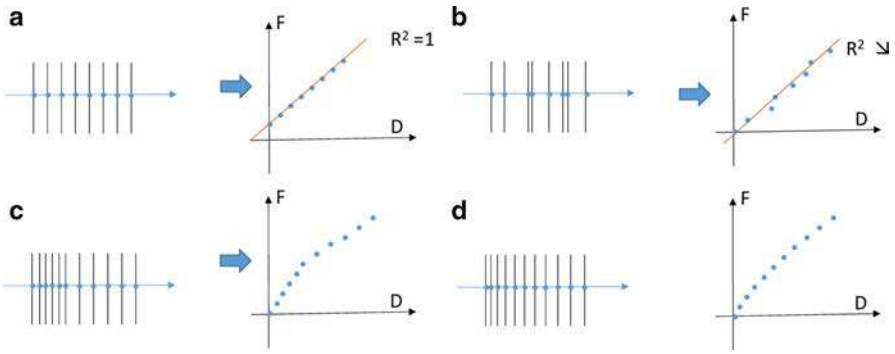

Fig. 3 Possible cases of (F, D) plots: **a** purely stationary, fractures are evenly organized. The coefficient of determination should be $R^2 = 1$; **b** not stationary. The mean value (i.e., slope) is the same but the coefficient of determination decreases; **c** abrupt change in fracture density. Residuals include trend; **d** gradual change in fracture density. The (F, D) plot shows an exponential-like shape, then residual should show cyclicity

3.2 Fracture Density Estimation

It is assumed that a $(F,\ D)$ graph is available over a given length, in which N_f fractures were counted. Let us consider that $(F,\ D)$ follows a linear trend. The aim is to estimate $P10$ as the slope $\hat{a}$ of the linear model between F and D as follows

$$f_i = \hat{a}.d_i + \hat{b} + \epsilon_i, i \in \{1, N_f\}. \tag{7}$$

The SR technique is used to estimate the slope $\hat{a}$. As mentioned in Sect. 2.1, a suitable model must be chosen. In the present case, the measured distance may contain errors, whereas the fracture rank is, by definition, controlled. Thus, although the interest for $P10$ computation is the derivative $\frac{\Delta F}{\Delta D}$ (i.e., the slope $\hat{a}$ of Eq. (7)), we propose to perform an LMS simple regression of D with respect to F. Hence, the estimated linear slope $\hat{a'}$ represents the inverse of the fracture density $\hat{d}_f$, expressed as follows

$$\begin{cases} d_i = \hat{a'}.f_i + \hat{b'} + \epsilon'_i, i \in \{1, N_f\} \\ \hat{d}_f = \frac{1}{\hat{a'}} \end{cases}. \tag{8}$$

Beyond the estimation of fracture density using the computed slope, the SR results present three additional interests (Fig. 3): (i) the coefficient of determination R^2 is a criterion for evaluating the representativness of $P10$ over the given range when it is stationary enough to be considered as constant over this range (Fig. 3a, b); (ii) the analysis of residuals highlights the cyclicity around the main linear trend and determines whether the linear model is appropriate (Fig. 3a, b); (iii) the estimated slope can be statistically compared with a slope (i.e., fracture density) estimated in another zone using the hypothesis testing presented in Sect. 2.2. This test checks whether the two values stem from the same population (i.e., similar fracture densities) or not (i.e, different fracture densities).

The first two points above are related to the study of the stationarity of $P10$ over the studied length. The third one is useful to compare $P10$ between different sampling zones. However, the hypothesis testing allows comparisons between two samples only. Multiple cross pairwise comparisons increase the risk $alpha$ (to reject H_0 although it is true). Therefore, an automated approach that uses the statistic t as a distance for clustering is proposed.

3.3 Automated Approach

Considering a fracture rank and cumulative distance dataset, the algorithm automatically identifies zones having the similar estimated $P10$. First, it divides the dataset into several zones. This needs to cut where fracture density drastically changes. Second, $P10$ is estimated for each zone as described in the previous section. Finally, a clustering algorithm is used to gather zones sharing statistically similar theoretical $P10$.

As previously stated (3.1), slope breaks in the $(F,\ D)$ graph correspond to sudden changes in fracture density. Slope variability may be characterized by the gradient,

which is the curvature (Fig. 3c) written as below

$$\text{grad}(a') = \frac{\text{d}a'}{\text{d}f}, \tag{9}$$

as

$$a' = \frac{\text{d}d}{\text{d}f}. \tag{10}$$

Then

$$\text{grad}(a') = \frac{\text{d}^2 d}{\text{d}^2 f} = \overrightarrow{k}(f), \tag{11}$$

where $\overrightarrow{k}$ is the curvature vector, whose norm is the curvature k. This suggests that abrupt changes in $P10$ are shown as high curvature values of the (F, D) graph. Therefore, the dataset is cut where the curvature k_j at a point j exceeds a given user-defined threshold. The dataset is thus divided into several non-overlapping zones. Two additional rules are accounted for: (i) each zone must contain at least three points; (ii) sucessive points with high curvatures are merged into a single zone. As a result, a set of N_p zones are generated. On each zone, $P10$ is estimated using the approach proposed in the previous section. For each zone $j \in [1; N_p]$, it provides two outputs: (i) the slope a'_j, then the $P10 = \hat{d_{fj}}$; (ii) the coefficient of determination R^2_j, revealing the local stationarity.

Moreover, the statistic t_{ij} is computed between each pairwise zone i and j. Instead of using the statistic t_{ij} for statistical comparison, t_{ij} is used as a distance between slopes of two parts: the lower t_{ij} is, the closer both slopes a'_i and a'_j are, hence d_{fi} and d_{fj}. A matrix of the distances t_{ij} between slopes a'_i and a'_j, $i, j \in [1; N_p]$ is built. Finally, an HAC clustering algorithm is used to gather zones sharing similar $P10$. The key point is to use the statistic t_{ij} as the clustering distance. In this paper, the "complete link" is used as the aggregation criterion.

Thus, the zones sharing the similar $P10$ according to t_{ij} are clustered into the same group. The resulting groups with a similar density may be spatially consecutive, or not.

4 Applications

A synthetic case study has been generated to test the performance of the approach for detecting fracture corridor boundaries. Then, a real case study is used to show the usefulness of characterizing fracture corridors from field data. The results of this method were then compared to the overall and visual interpretations of a structural field geologist.

4.1 Synthetic Dataset

A three-dimensional $100 \times 100 \times 50u^3$ grid was built with a resolution of $1u$ (u is a given reference unit). Three zones have been generated (Fig. 4): the diffuse fractures (FD), the first ($FC1$) and the second ($FC2$) corridors.

Whithin the grid, discrete fracture networks were generated using a stochastic simulation algorithm available in Gocad-SKUA software. Fractures were simulated as rectangles using a Poisson-point process (Goovaerts 1997). Input parameters are probability laws for fracture sizes and orientations. This algorithm relies on an intensity parameter θ, which is physically similar to $P30$.

First, fracture sets were defined as DF, $FC1$ and $FC2$ networks. To avoid the effect of fracture orientation variabilities, all fractures were assumed to be vertical (dip$= 90°$) and $N000$-trending. Fracture size was similar for all sets. The fracture width was defined as a uniform density probability law (pdf) ranging from 20 to 30. Fracture height was a constant width-height ratio equal to 2. Only densities varied between zones and were equal to $1.e^{-4}$ fractures$/u$ for FD, to $1.e^{-3}$ for $FC1$ and to $2.e^{-3}$ for $FC2$. Fracture corridors have densities at least 10 times higher than diffuse fractures (Chatelée et al. 2015).

Second, 100 scanlines were simulated. A hundred straight lines were simulated perpendicularly to the fracture strikes between $X = -10u$ and $X = 110u$ so they crossed the entire grid. Their Y and Z locations were randomly chosen using a Monte-Carlo sampling technique on uniform laws conditioned to respective grid dimensions.

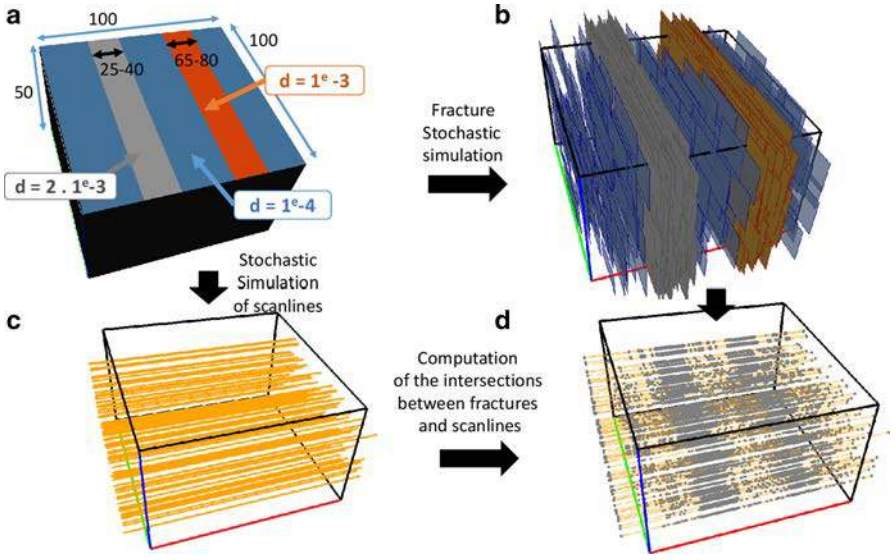

Fig. 4 Stochastic simulations of fracture corridors: **a** the different zones, the diffuse fractures (FD, blue), the first corridor ($FC1$, orange), and the second one ($FC2$, grey); **b** a realization of the stochastic simulation of fractures; **c** stochastic simulation of 100 scanlines; **d** Computation of the intersection points between the fractures and the scanlines. Each point corresponds then to an observed fracture

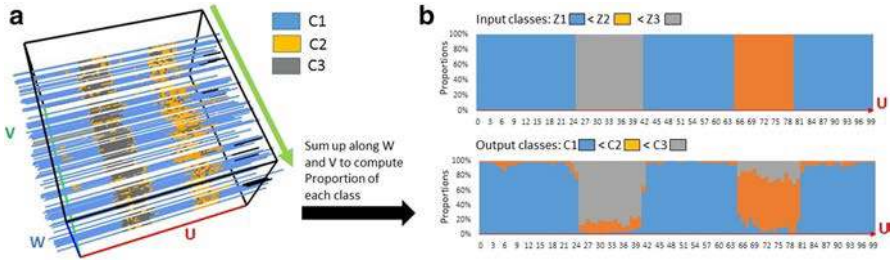

Fig. 5 Results of the classification: **a** the resulting zones mapped along the 100 scanlines. The three classes are ordred after the estimated densities such as $C_1 < C_2 < C_3$; **b** Results of the cumulative computation of the proportions of each class along the V axis. Top: the input zones with lower density in diffuse fracture zones (Z1, blue), the first fracture corridor (Z2, orange), the second one (Z3, grey). Bottom: the proportions of the three classes

The sampling for proportion computation was performed at 15 in Y and 7.5 in Z from the grid boundaries to avoid border effects.

Third, the scanlines were cut by all the fracture surfaces. Each time a scanline was intersected by a surface, a point was added to the polyline. From -10 to 110, the cumulative distance D at a point and rank F were computed so that 100 scanlines with variables D and F were obtained.

The procedure was applied on the 100 scanlines (Fig. 5). Three classes were found, namely $C_1 < C_2 < C_3$. The computed $P10$ could not be compared to the input $P30$ because they are different entities. However, it was observed in the three-dimensional view of the scanlines (Fig. 5a) that the trend of the input densities was reproduced and that the fracture corridor boundaries had been detected. In Fig. 5b, the cumulative proportions of each class were summed up along the **V** axis. The input DF, $FC1$, and $FC2$ zones were detected, on average. It may be noticed that the proportion of the lower density was greater in $FC1$ than in $FC2$. This was consistent with the input data as $FC1$ had a lower density than $FC2$.

4.2 Case Study

The Calvisson quarry (Cévennes Massif Lat. 43.786551, Long. 4.172987; Southern France) was chosen as a case study for analyzing fracture corridors because the quarry exposes high-quality and continuous outcrops on walls at two of its levels. This allows the corridors to be observed continuously and in three dimensions (Fig. 6a). The host rocks are limestones of Lower Hauterivian age (Berger 1974), gently dipping 15° to 20° to the north. The fracture network is composed of diffuse fractures (Fig. 6c) alternating with localized corridors (Fig. 6b, d). The main diffuse fracture set trends SW-NE and a minor set trends NW-SE. Fracture corridors are 2 to 10 meters wide and 20 to 200 meters distant from each other. The geometrical analysis allows to the identification of 10 corridors that are visible on 19 sites along both quarry levels, 8 of them striking NE-SW (Bisdom et al. 2014; Chatelée et al. 2015). Fracture measurements were acquired along three scanlines located on Fig. 6. Scanline 1 (SL1) was measured on level 2, along 25.81 meters from south to north and crossing a fracture corridor. The corridor

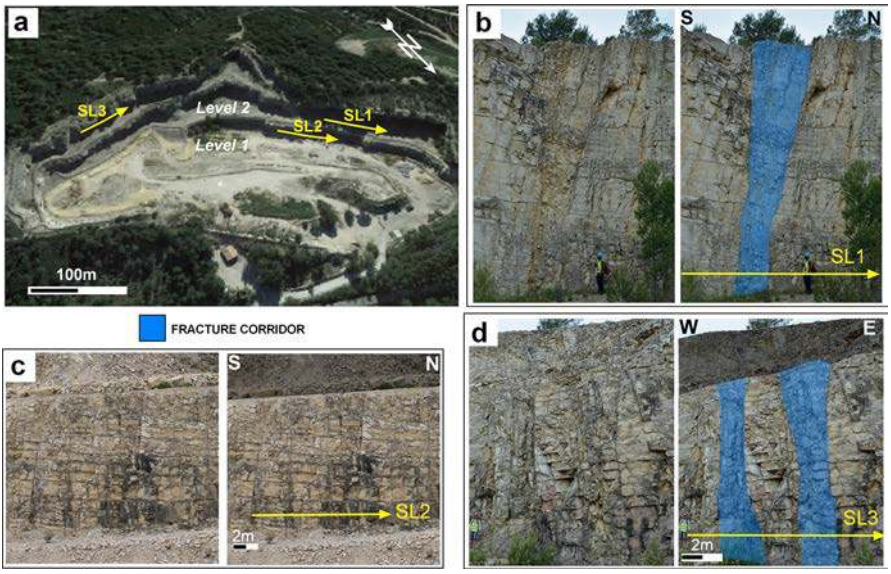

Fig. 6 Photographs of the case study quarry of Calvisson (Cévennes Massif Lat. 43.786551, Long. 4.172987; Southern France). **a** Aerial picture of the quarry and location of 3 sampled scanlines; **b** scanline 1 (SL1) crossing though a single fracture corridor; **c** scanline 2 (SL2) across diffuse fractures; **d** scanline 3 (SL3) crossing through a dual zone fracture corridor

is composed of breccias and dense fractures (Fig. 6b). Scanline 2 (SL2) was measured on level 1, along 20.42 meters from south to north and crossing diffuse fractures only (Fig. 6c). Scanline 3 (SL3) was measured on level 2 along 24.27 meters from west to east. This scanline crosses, from west to east, a fractured corridor composed of two densely fractured zones bracketing an intact zone (Fig. 6d), and a blast zone related to quarrying operations. Along the scanlines, the fractures are numbered from 1 to 347 in SL1, from 1 to 211 in SL2 and from 1 to 287 in SL3. For each fracture, the spacing to the previous fracture is measured and the distance to the first fracture is then computed. The Terzaghi correction has been applied to correct the fracture spacing.

The above proposed approach was applied to each scanline. The achieved dendrogram of density separation is displayed on Fig. 7. The number of density groups of each scanline is deciphered by a cut threshold at the second highest distance separation (red dashed line on Fig. 7). On SL1 and SL3, three groups of density range (G1 to G3) are obtained and four groups on SL2 (G1 to G4). R^2 was also computed for each scanline zone and the minimum, maximum and average values of R^2 per cluster and per scanline are shown in the Table 1. As the clusters G3 of SL1 and SL3 and the cluster G4 of SL2 are singletons, the single computed value is set in the row of the average of R^2 only.

The density groups are displayed as a color scale along each scanline. The scanlines are positioned on the photos in front of their corresponding outcrop (Fig. 8) where fracture corridors detected with the human eye are painted blue. The SL1 is composed of three density groups. Along the line, tow areas are distinguished: the southern half

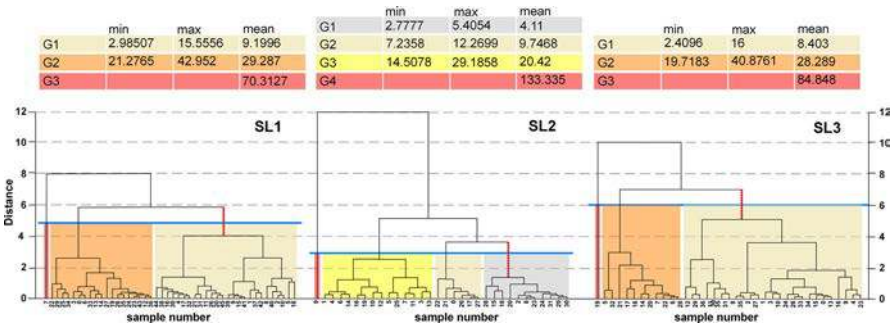

Fig. 7 Graphical ouput of dendrogram analysis of density groups separation applied on scanlines SL1, SL2 and SL3. Horizontal scale: number of the scanline segment; vertical scale: distance separation between two density groups. The number of density groups results from a cut at the second highest distance separation (red dashes line). The min-max and mean fracture density for groups G1 to G4 is given in tables and colored from grey to red from lower to higher density

of the line is dominated by group 1 densities (G1, beige on Fig. 8) and corresponds to diffuse fractures in the outcrop; the northern half is dominated by group 2 densities (G2, orange on Fig. 8) and fits with the fracture corridor. A minor high-density group (G3, red on Fig. 8) corresponds to a local, confined and neglectable high fracture density. The area dominated by high density is slightly larger than the fracture corridor detected by human eyes. Indeed, the proposed approach allows to overcome the bias inferred by human judgement and a priori on fracture density estimation. The SL2 is composed of four groups. With exception of group 4, which is anecdotic, the relative low gaps on the dendrogram (Fig. 7) between groups G1 to G3 show that these three groups are not so differentiated. These groups are randomly distributed along the scanline where only diffuse fractures occur (Fig. 8, SL2). The SL3 is composed of three groups of density. G3 is an outlier but fits anyway in a fracture corridor. Density groups G2 and G3 are well differentiated on the dendrogram of Fig. 7. When compared to the outcrop, the highest and medium density groups fit perfectly with the location of the dual fracture corridor and of a blast zone (respectively blue and green on Fig. 8). The low-density group G1 is located along areas of diffuse fractures.

The R^2 values obtained per group are all very high. They are rougly always greater than 0.8, except for G2 of SL1 (minimum is 0.6693) and G1 of SL2 (minimum is 0.747). This shows that the fracture spacing is particularly stationary in each zone.

To summarize the fracture density analysis, the dendrograms show either well or poorly differentiated density groups, which corresponded respectively to outcrops with or without fracture corridors. In addition, the location of high density groups fit with the observed corridors on the outcrop. In the case of SL1, the fracture analysis detected a wider density increase, which the human eye did not arbitrarily notice. Finally, when local anomalous high density occurs along a line (group G3), it is not misinterpreted and does not influence the detection of fracture corridors.

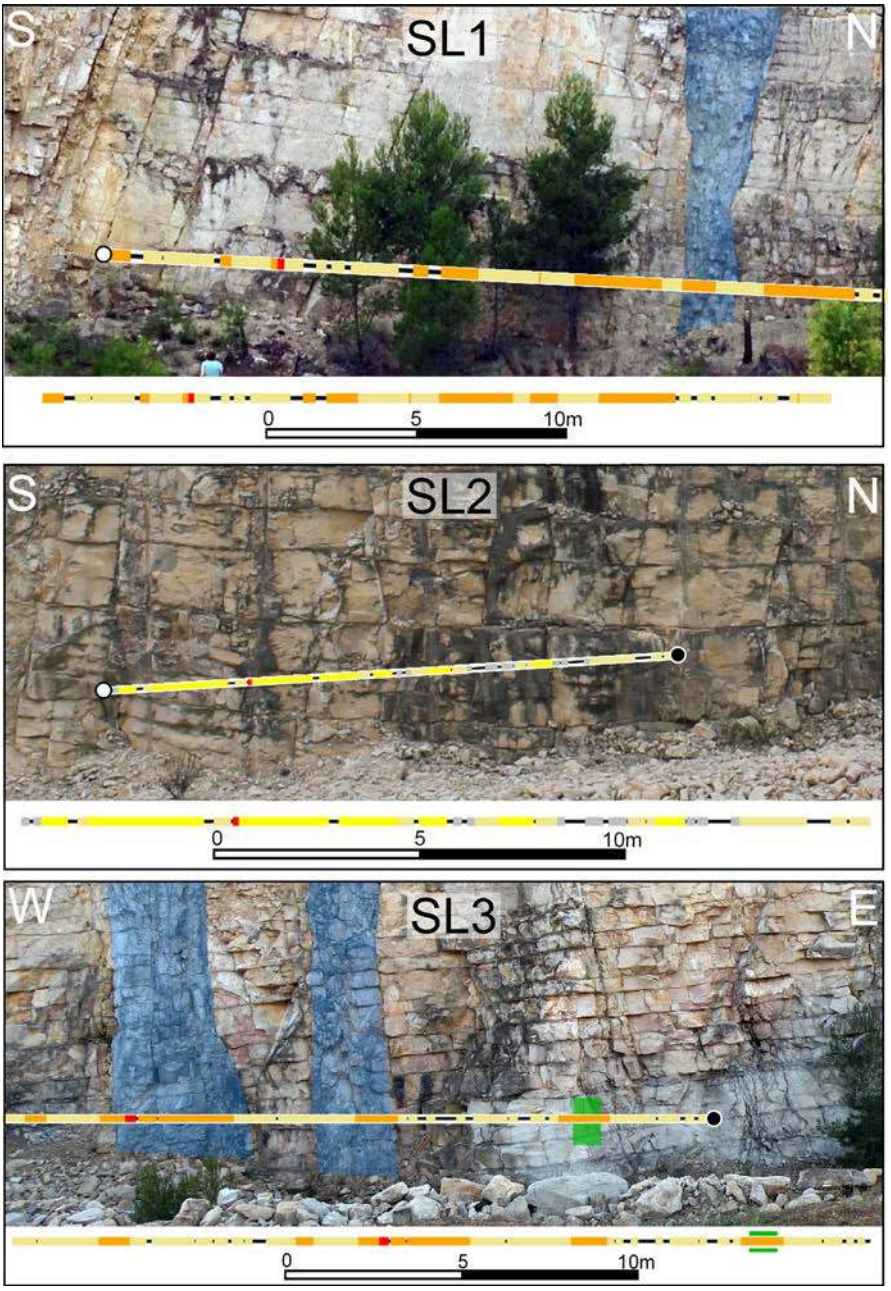

Fig. 8 Comparison of density group analysis on scanlines with the outcrops. Color scale after Fig. 7

Table 1 Resulting minimum, maximum and average R^2 per cluster and per scanline, except for G4 of SL2 and G3 of SL1 and SL3, in which only a single scanline zone is contained. Then, the single value is given in the average R^2 line

–	SL1			SL2				SL3		
Cluster	G1	G2	G3	G1	G2	G3	G4	G1	G2	G3
Minimum R^2	0.7946	0.747	–	0.6693	0.8359	0.8439	–	0.8369	0.8848	–
Maximum R^2	0.9995	0.99	–	0.9999	0.9999	0.9888	–	0.9997	0.9789	–
Average R^2	0.9415	0.927	0.9024	0.88985	0.9351	0.9252	0.9868	0.9645	0.9508	0.9758

5 Conclusions

The proposed approach not only estimates the fracture density, but also compares fracture densities within or between datasets. This approach is based on the analysis of FCI curves computed from well data or scanlines. The key idea is to combine regressions with hypothesis testing and clustering in order to propose a formal approach to decipher regions with different fracture densities. Beyond the computation of fracture density, this technique allows: (i) criteria to be defined for evaluating the stationarity of the fracture density over the given range and whether this fracture density is statistically representative for this range; (ii) the typology of fracture density to be defined as a function of the derivative variability.

The results show that this approach has the ability to detect the boundaries of zones with a specific fracture density. The use of the curvature threshold provides the possibility of fitting other models than linear ones. In the case of linear fitting, it could be also interesting to check if it is possible to combine piecewise linear regression with the hypothesis testing. Another possibility could be to combine this approach with the lacunarity method. Indeed, lacunarity provides information about the sizes and spacings of fracture pattern clusters. This information could be used to guide the splitting of FCI curves, in addition to the curvature value.

Other applications of this approach are envisaged in order to compare fracture densities obtained from different data sources or facies. The proposed technique can also be used to statiscally compare values between any known region boundaries. Further investigations may focus on the use of this approach on different case studies, especially on well data from petroleum subsurface data. The statistical framework of the approach could also be useful for correlations between well data and other subsurface data, such as seismic. Finally, this approach can be applied to any fractured reservoir problematic, which includes petroleum or water ressources and CO_2 or nuclear waste storage.

Acknowledgements The authors would like to thank the ParadigmGeo company and the ASGA for their support in providing the gOcad software and, respectively, its research plug-ins. The field data were acquired thanks to the BICARBOFRAC project granted by Total S.A.

References

Agosta F, Alessandroni M, Antonellini M, Tondi E, Giorgioni M (2010) From fractures to flow: a field-based quantitative analysis of an outcropping carbonate reservoir. Tectonophysics 490(3–4):197–213

Antonellini M, Aydin A (1994) Effect of faulting on fluid flow in porous sandstones: petrophysical properties. AAPG Bull 78:355–377

Barthélémy J, Guiton L, Daniel J (2009) Estimates of fracture density and uncertainties from well data. Int J Rock Mech Min Sci 46:590–603

Berger G (1974) Carte géologique de sommières. In: Carte géologique de la France à 1:50 000. 964, Sommières, GRGM

Bisdom K, Gauthier B, Bertotti G, Hardebol N (2014) Calibrating discrete fracture-network models with a carbonate three-dimensional outcrop fracture network: implications for naturally fractured reservoir modeling. AAPG Bull 98(7):1351–1376

Bonneau F, Henrion V, Caumon G, Renard P, Sausse J (2013) A methodology for pseudo-genetic stochastic modeling of discrete fracture networks. Comput Geosci 56:12–22

Chatelée S, Lamarche J, Gauthier B (2015) Fracture corridors in carbonates. In: 77th EAGE conference and exhibition 2015 earth science for energy and environment, Madrid, Spain
Chilès JP (1988) Fractal and geostatistical methods for modeling of a fracture network. Math Geol 20(6):631–654
Dershowitz W (1984) Rock joint systems. phdthesis, Massachusetts Institue of Technology, Cambridge
Dershowitz W, Herda H (1992) Interpretation of fracture spacing and intensity. In: 33rd US symposium on rock mechanics. Santa Fe, NM, pp 757–766
Dezayes C, Valley B, Maqua E, Syren G, Genter A (2005) Natural fracture system of the soultz granite based on ubi data in the gpk3 and gpk4 wells. In: EHDRA scientific conference, pp 17 – 18
Eisenhauer JG (2003) Regression through the origin. Teach Stat 25(3):76–80
Emiliano D, nos Rodríguez B, Altamira-Areyán A (2016) Static fracture distribution model based on sedimentary facies. In: AAPG international convention and exhibition
Fox A, Pointe PL, Hermanson J, Ohman J (2007) Statistical geological discrete fracture network model. Forsmark modelling stage 2.2 R-07-46, SKB
Gauthier BDM, Bisdom K, Bertotti G (2012) Modeling 3d fracture network in carbonate nfr: contribution from an analogue dataset, the cante perdrix quarry, calvisson, se france. In: AAPG Hedberg conference
Gauthier B, Franssen R, Drei S (2000) Fracture networks in rotliegend gas reservoirs of the dutch offshore: implications for reservoir behaviour. Netherlands J Geosci 79(1):45–57
Gillespie P, Howard C, Walsh J, Watterson J (1993) Measurement and characterisation of spatial distributions of fractures. Tectonophysics 226:113–141
Gillespie PA, Johnston JD, Aand LKJM, McCaffrey WJJ, Watterson J (1999) Influence of layering in vein systematics in line samples. Fract Fluid Flow Miner Geol Soc Spec Publ 155:35–56
Goovaerts P (1997) Geostatistics for natural resources evaluation. Oxford University Press, Oxford
Hansford J, Fishe Q (2009) The influence of fracture closure from petroleum production from naturally fractured reservoirs: a simulation modelling approach. In: AAPG annual conference and exhibition
Jambayev A (2013) Discrete fracture modeling for a carbonate reservoir. Master's thesis, Colorado School of Mines
Kherroubi J, Etchecopar A (2009) Fracture characterization from borehole image: a quantified approach. In: AAPG annual conference and exhibition
Marrett R, Gale JF, Gómez LA, Laubach SE (2018) Correlation analysis of fracture arrangement in space. J Struct Geol 108:16–33
Narr W, Suppe J (1991) Joint spacing in sedimentary rocks. J Struct Geol 13(9):1037–1048
Ray SD, Al-Shammeli A, Verma NK, Matar S, de Groen V, de Joussineau G, Ghilardini L, Le Maux T, Al-Khamees W (2012) Characterizing and modeling natural fracture networks in a tight carbonate reservoir in the middle east: a methodology. Bull Geol Soc Malays 58:29–35
Roy A, Perfect E, Dunne WM, Odling N, Kim JW (2010) Lacunarity analysis of fracture networks: evidence for scale-dependent clustering. J Struct Geol 32:1444–1449
Roy A, Perfect E, Dunne WM, McKay LD (2014) A technique for revealing scale-dependent patterns in fracture spacing data. J Geophys Res Solid Earth 119:5979–5986
Saporta G (1997) Probabilité. Editions Technip, Analyse de données et statistique
Souche L, Ghorayeb K, Belova N, N QD (2016) Innovative approach for building and calibrating multiple fracture network models for fractured carbonate reservoirs. In: SPE annual technical conference and exhibition, SPE-181584-MS
Terzaghi R (1964) Source of error in joint surveys. Geotechnique 15:287–304
Tokhmchi B, Memarian H, Rezaee M (2010) Estimation of the fracture density in fractured zones using petrophysical logs. J Pet Sci Eng 72:206–213